

Experimental test of theories describing the magnetic ac susceptibility of differently shaped superconducting films: Rectangles, squares, disks, and rings patterned from $\text{YBa}_2\text{Cu}_3\text{O}_{7-\delta}$ films

Th. Herzog, H. A. Radovan, and P. Ziemann

Abteilung Festkörperphysik, Universität Ulm, D-89069 Ulm, Germany

E. H. Brandt

Max-Planck-Institut für Metallforschung, Institut für Physik, D-70506 Stuttgart, Germany

(Received 10 December 1996)

The magnetic ac response of rectangles, squares, disks, and rings patterned from $\text{YBa}_2\text{Cu}_3\text{O}_{7-\delta}$ films (typical thickness 200 nm) was determined as a function of temperature for the case of the exciting external magnetic ac field being directed perpendicular to the film plane. For this geometry strong demagnetizing effects are expected and corresponding theories describing the resulting real (χ') and imaginary (χ'') parts of the magnetic susceptibility χ on the basis of critical state models have only recently been developed. Plotting χ'' versus χ' turns out to be useful in order to test these theories with respect to different sample shapes without invoking a specific temperature dependence of the critical current density $J_c(T)$. In this way, the following results were found. The shape dependent differences of the susceptibility are only small (of the order of %) with the smallest difference between squares and disks as predicted by theory. The recent theories yield an improved description of the experimental χ data as compared to a conventional Bean model neglecting demagnetization effects. At temperatures just below the superconducting transition, however, these theories based on purely hysteretic losses fail to be quantitative. A systematic change of symmetry of the χ'' versus χ' curves is observed if rings of decreasing widths are patterned from a disk. For a diameter to width ratio $D/w > 20$ the experimental susceptibilities, including the temperature dependence of the third harmonic, approach the behavior as calculated for an ideal thin narrow ring. This result allows a quantitative determination of $J_c(T)$ on such rings as is demonstrated by additional dc magnetization measurements using a SQUID magnetometer. [S0163-1829(97)04729-2]

I. INTRODUCTION

The discovery of high- T_c superconductors (HTSC's) has led to a remarkable upsurge in interest in techniques allowing a contact free characterization of superconducting properties like the transition temperature T_c or the critical current density J_c . Among the different technical approaches, the measurement of the magnetic susceptibility χ became the most popular for various reasons, one being its experimental simplicity, at least for bulk samples. Another important reason was the broad basis of experience resulting from the previous application of different variants of this technique to characterize conventional superconductors. Especially for type-II superconductors it had been demonstrated that a combination of an external magnetic dc field with a susceptibility measurement allows one to determine the spatial distribution of the penetrating dc field.¹ These measurements turned out to be especially useful to test models describing the hysteretic magnetization observed for the technically relevant superconductors with strong pinning. Such models, the most popular being due to Bean² and Kim-Anderson,³ in principle allow one to calculate the magnitude of the magnetization \mathbf{M} as a function of the external magnetic field \mathbf{H} . If an ac field H_{ac} is applied, Fourier transformation of the resulting time dependent magnetization $\mathbf{M}(t, H_{ac})$ yields the real and imaginary parts of the susceptibility $\chi'(\omega)$ and $\chi''(\omega)$, respectively.⁴ In practice, however, the model predictions were restricted to simple and idealized sample shapes and

field orientations, for which demagnetization effects could be excluded or neglected.⁵ Well-known examples are the infinite cylinder or the infinite slab geometry with the field parallel to the long extension. Thus, at the advent of HTSC, the susceptibility technique already was quite mature, including also the awareness of some possible pitfalls of this method.⁶

Since the imaginary part of the susceptibility allows one to monitor losses caused by a time variation of vortex configurations, corresponding measurements seem to be especially suited to characterize HTSC samples either with respect to their quality or to the basic loss mechanisms. Much effort was devoted to this latter aspect in the context of the so-called irreversibility line; representative contributions to this issue can be found in Ref. 7. More recently, it became clear from both theoretical as well as experimental insights how complex the behavior of HTSC vortex systems can be. This resulted in a further motivation to apply susceptibility techniques for studying loss phenomena related to, e.g., thermally assisted flux flow (TAFF), giant flux creep, vortex glass phases, as well as a possible melting of the vortex system. All these phenomena lead to a richness of transition lines in the H - T phase diagrams describing the HTSC vortex systems, and they still remain a challenge to theory, the state of the art of which has been reviewed recently.⁸

Parallel to the development of theoretical concepts describing HTSC vortex systems, much progress has also been achieved in predicting the electromagnetic response of conventional type-II superconductors in the case of more complicated sample shapes.⁹ In particular, for thin films the prob-

lem of finite rectangular strips and circular disks in a magnetic field oriented perpendicular to the surface has been theoretically addressed.^{10–15} As a result, for these geometries the real and imaginary parts of the susceptibility can be calculated as a function of the applied magnetic field. It turns out that the problem can be parametrized by normalizing the driving field H_{ac} to the penetration field H_p which, as in the Bean model for simple geometries, is proportional to the critical current density $J_c(T)$ with the proportionality coefficient being determined by the geometrical length scales of the sample. Thus, if the theory is tested by plotting the imaginary versus the real part of the susceptibility, there should be no difference whether the experimental data were obtained by a variation of the field H_{ac} or of the temperature. This prediction is verified below.

The main aim of the present paper is to check the general agreement between the theoretical predictions of $\chi''(\omega)$ versus $\chi'(\omega)$ relations for different geometries, which are all based on Bean-like hysteretic losses, with experimental data that may include additional loss mechanisms like flow or flux creep. Special emphasis is put on the sensitivity of the experimental results to systematic changes of the geometry. For example, theory predicts only small differences of the order of 1% between the magnetic moments of thin strips and disks as a function of the applied magnetic field if normalized to the same initial slope and saturation value. The predicted difference should be even smaller when comparing squares and disks in the same way. Both predictions are confirmed by our experiment.

On the other hand, it will be demonstrated that thin superconducting rings behave significantly different from disks of the same outer diameter. To study this effect in more detail, a thin YBaCuO disk (outer diameter 1 mm) was sequentially patterned to rings of varying width (from 400 to 50 μm). In this way it could be shown how the experimental results approach the behavior predicted by a simple model describing the response of a superconducting idealized narrow ring of a given inductance L , which is determined by its radius R and width w . Additional data will be presented indicating the influence of changing R and w independently. In the limit of an idealized ring, the susceptibility data allow an accurate determination of the critical current density $J_c(T)$; this conclusion is corroborated by comparison to results obtained by dc-magnetization measurements on the same ring in a SQUID magnetometer. Finally, for such a ring with a well-defined value of $J_c(T)$, the model allows one to calculate the real and imaginary parts of the third harmonics $\chi'_3(T)$ and $\chi''_3(T)$. For the latter quantity a pronounced structure is predicted in agreement with the experimental results for narrow rings as opposed to full disks.

II. EXPERIMENTAL DETAILS

All results reported in this work were obtained on photolithographically patterned $\text{YBa}_2\text{Cu}_3\text{O}_{7-\delta}$ films. These films were prepared by cylindrical magnetron sputtering using a stoichiometric YBaCuO ring target.^{16,17} Deposition onto (100)oriented SrTiO_3 single crystals under optimized conditions in all cases resulted in epitaxially grown $\text{YBa}_2\text{Cu}_3\text{O}_{7-\delta}$ films with their c -axis parallel to the substrate normal as revealed by x-ray diffractometry (XRD).

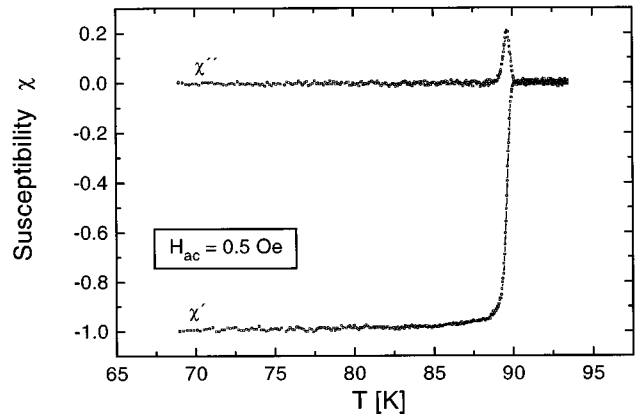


FIG. 1. Temperature dependence of the real (χ') and imaginary (χ'') parts of the susceptibility χ of a typical $\text{YBa}_2\text{Cu}_3\text{O}_{7-\delta}$ film as used in the present work.

The rocking angles of the films varied between 0.1° and 0.3° , indicating state of the art epitaxial quality. Similarly, the c -axis lattice parameters given by XRD from Θ - 2Θ scans point to nearly stoichiometric films ($\delta \approx 0$).

The ac susceptibility is determined in a susceptometer especially designed for measurements on thin films. The details of this apparatus are described in Ref. 18. In short, the samples are fixed to a sapphire lever mounted at the bottom of a He cryostat. This lever can be rotated from outside under computer control around a sapphire axis, onto which a heater and a thermometer is mounted. The rotation allows the sample to be positioned into the gap of a split coil (Helmholtz arrangement) providing the excitation field H_{ac} , while a pickup coil above the sample monitors its magnetic response applying a lock-in technique. The good thermal conductivity of the sapphire parts, on the other hand, enables a controlled variation of the sample temperature between 5 K and 300 K. In this way, the temperature dependence of the real and imaginary parts of the susceptibility, $\chi'(T)$ and $\chi''(T)$, can be determined for different values of H_{ac} . For the present measurements, the frequency of H_{ac} was fixed at 1042 Hz. In addition to the fundamental susceptibility, the real and imaginary parts of the third harmonic, $\chi'_3(T)$ and $\chi''_3(T)$, could be detected. It is important to note that due to the special position of the samples relative to the external magnetic field and the pickup coils, we determine in all cases their magnetic response to the component of the external field perpendicular to the substrate.

This ac-susceptibility technique was also applied before patterning the $\text{YBa}_2\text{Cu}_3\text{O}_{7-\delta}$ films in order to characterize their superconducting properties, especially the transition temperature T_c as well as the phase purity. An example is presented in Fig. 1, where the temperature dependence of the real and imaginary parts of a YBaCuO film is shown, obtained by applying a field of $H_{ac} = 0.5$ Oe. Defining T_c by the temperature corresponding to the first significant (1%) deviation of $\chi'(T)$ from zero, a value of $T_c = 90.0$ K is obtained, which is representative for all films used in the present study. For temperatures below $T_c - \delta T_c$, where the transition width δT_c is of the order of 1 K, the imaginary part $\chi''(T)$ indicating losses is zero, and the signal of the real part $\chi'(T)$ is normalized to -1 corresponding to ideal diamagnetic behavior. Previous experience shows that a struc-

tureless sharp transition of the ac susceptibility is a strong criterion for good quality superconducting samples, allowing one to exclude multiple phases with varying T_c values.¹⁹ In the present work only $\text{YBa}_2\text{Cu}_3\text{O}_{7-\delta}$ films passing this criterion were used.

For patterning the films, a combination of lithography using a positive photoresist and wet chemical etching with 2% phosphoric acid or EDTA was applied. The resulting slow etching rate allows the continuous control of the etching progress by optical confocal microscopy. This control guarantees that etching is complete, a point which is especially important for the inner part of patterned ring structures. To study the influence of sample geometry for one and the same film, a disk with an outer diameter of 1 mm was patterned first and, after ac-susceptibility measurements, different ring masks were carefully aligned allowing one to prepare rings with widths varying between 400 μm and 50 μm . For rings with even smaller widths (25 μm and 10 μm) proper alignment turned out to be difficult and these rings were prepared from different starting films.

III. RESULTS AND DISCUSSION

A. Rectangles, squares, and disks

The magnetic moment $\mathbf{m} = \frac{1}{2} \int \mathbf{r} \times \mathbf{J}(\mathbf{r}) d^3r$ of a type-II superconductor is often calculated within the Bean model,^{2,5} which assumes that the current density $\mathbf{J}(\mathbf{r})$ cannot exceed a critical value J_c , $J = |\mathbf{J}| \leq J_c$. If J locally exceeds J_c , the flux lines will rearrange such that $J \leq J_c$ again holds in the entire superconductor. An additional assumption disregards the reversible magnetization, or the finite lower critical field H_{c1} , by writing $\mathbf{B} = \mu_0 \mathbf{H}$ inside (and outside) the material. Within this model, \mathbf{m} depends only on the applied magnetic field H_a and on the geometry, i.e., on the sample shape and on the orientation of H_a . A general consequence of the Bean assumption of a field-independent J_c is that the virgin curve $m(H_a)$ (with H_a increased from zero) determines the full hysteresis loop of m when H_a is cycled between $-H_0$ and $+H_0$. The branches m_\downarrow and m_\uparrow in decreasing and increasing H_a read

$$m_\downarrow(H_a, H_0) = m(H_0) - 2m \left(\frac{H_0 - H_a}{2} \right),$$

$$m_\uparrow(H_a, H_0) = -m(H_0) + 2m \left(\frac{H_0 + H_a}{2} \right). \quad (1)$$

We list some basic examples for virgin magnetization curves. A large superconducting slab of width $2a$ and area A , and a long cylinder with radius a and length l , in a *parallel* field have the magnetic moments^{2,5}

$$m_{\text{slab}} = -J_c a^2 A (2h - h^2), \quad (2)$$

$$m_{\text{cyl}} = -\pi J_c a^3 l (h - h^2 + h^3/3) \quad (3)$$

for $0 \leq h \leq 1$ with $h = H_a/H_p$, where $H_p = J_c a$ is the field of full penetration. For $H_a \geq H_p$, or $h \geq 1$, m stays constant since the current density has saturated to $J = J_c$ in the entire sample.

A thin strip^{10–12,20} of width $2a$ and length $l \gg a$ and a circular disk^{13–15} of radius a , both with thickness $d \ll a$, in a transverse field H_a have the magnetic moments

$$m_{\text{strip}}(H_a) = -J_c d a^2 l \tanh h, \quad (4)$$

$$m_{\text{disk}}(H_a) = -J_c d a^3 \frac{2}{3} \left(\cos^{-1} \frac{1}{\cosh h} - \frac{\sinh|h|}{\cosh^2 h} \right) \quad (5)$$

for $0 \leq h < \infty$ with $h = H_a/H_c$, where $H_c = J_c d/\pi$ for the strip and $H_c = J_c d/2$ for the disk. The two curves (4) and (5) differ only by 0.012 if normalized to the same initial slope $m'(0)$ and same saturation value $m(\infty)$. The computed normalized Bean magnetic moment $m_{\text{square}}(H_a)$ for a thin superconducting square^{9,21,22} differs from $m_{\text{disk}}(H_a)$ by only 0.002.

In the considered limit $d/a \rightarrow 0$, the transverse moments $m_{\text{strip}}(H_a)$ and $m_{\text{disk}}(H_a)$ saturate only at infinitely large field H_a . With finite thickness d the magnetic saturation is reached when the flux and current front, which is positioned at $x_p = r_p = a/\cosh h$, has penetrated to a distance $\approx d/2$ from the center $x=0$ or $r=0$, i.e., to $x_p = r_p \approx d/2$. More precisely, one finds from analytic calculations²³ the penetration fields²⁴ for $d \ll a$,

$$H_p^{\text{strip}} = J_c \frac{d}{\pi} \left[1 + \ln \frac{2a}{d} \right], \quad (6)$$

$$H_p^{\text{disk}} = J_c \frac{d}{2} \left[2 + \ln \frac{2a}{d} \right]. \quad (7)$$

The prefactors in Eqs. (6) and (7) are the above-defined critical fields of strips and disks, $H_c = J_c d/\pi$ and $H_c = J_c d/2$. Above the penetration fields (6) or (7) the magnetic moment saturates to the values $m_{\text{sat}}^{\text{strip}} = J_c d a^2 l$ and $m_{\text{sat}}^{\text{disk}} = J_c d a^3 \pi/3$.

The experimental behavior of a rectangle (size $2 \times 3 \text{ mm}^2$) and a disk (diameter 1 mm), both made out of the same YBaCuO film, is shown in Fig. 2, where the temperature dependence of the corresponding real and imaginary parts of the susceptibility are presented for a series of different exciting fields H_{ac} . The typical trend that the maximum of χ'' is shifted to lower temperatures for increasing field amplitudes can clearly be seen for both sample shapes. Within a Bean model, the maximum of χ'' is attained at a temperature T_{max} , at which the applied field amplitude H_{ac} approaches the penetration field H_p of the corresponding sample geometry, i.e., for $H_{ac} = H_p(T_{\text{max}})$. The scaling of H_p with $J_c(T)$, which is expected to be a monotonically increasing function for decreasing temperatures, immediately leads to the observed shift of T_{max} to lower values. Once the external field exceeds H_p at a fixed temperature, or, as in the present ac measurement, at temperatures $T < T_{\text{max}}$ for a fixed amplitude H_{ac} , the sample's magnetic moment approaches saturation and the susceptibility decreases, respectively.

Another general trend found for the susceptibility curves presented in Fig. 2 is the developing asymmetry of the χ'' peaks towards lower temperatures for increasing amplitudes H_{ac} accompanied by a corresponding broadening of the $\chi'(T)$ transition. This behavior reflects the temperature dependence of an effective lower critical field H_1 , above which the ac-field penetrating the sample produces losses. In prin-

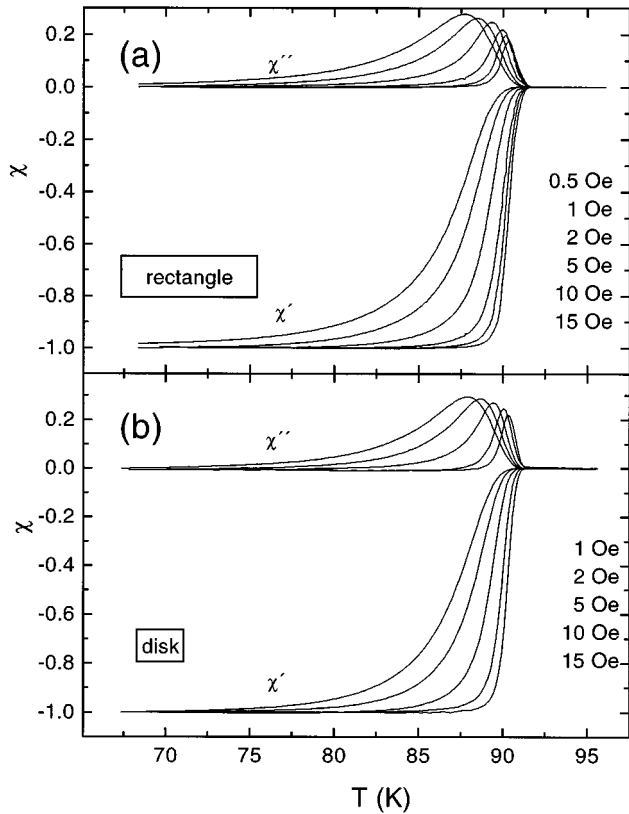


FIG. 2. Influence of the effective magnetic ac field as given in the insets on the temperature dependence of the susceptibilities of (a) a rectangle of $2 \times 3 \text{ mm}^2$ and (b) a disk of diameter 1 mm, both patterned from a YBaCuO film.

ciple, H_1 can be determined by referring to a criterion like $H_1(T^*) = H_{ac}$, where T^* is the onset temperature for losses as given by the first significant deviation of $\chi''(T)$ from zero (e.g., 10% above the low temperature noise level). For samples and field orientations for which demagnetization effects can be neglected, H_1 could be identified with the lower critical field H_{c1} .²⁵ Clearly, due to the monotonic increase of H_1 for decreasing temperatures, for increasing amplitudes H_{ac} , T^* is shifted to lower values. For temperatures below T^* , the samples are perfectly screened by supercurrents with corresponding susceptibility values of $\chi''=0$ and $\chi'=-1$. For decreasing amplitudes H_{ac} , the temperature T^* approaches T_c and perfect screening is observed for all $T \leq T^*$. In this case, the χ'' peak may be interpreted as a δ function²⁶ broadened due to a nonideal transition into the superconducting state as well as due to nonperfect electronics rather than as being caused by a hysteretic or viscous loss mechanism. This interpretation is confirmed by earlier measurements on Pb foils of similar shape. These type-I superconductors exhibit χ'' peaks of identical heights for small amplitudes $H_{ac} (< 1 \text{ Oe})$.²⁷

There is another point worth mentioning. Within the Bean model, the height of the χ'' peak is independent of the amplitude H_{ac} . Comparison to Fig. 2 shows that such a behavior is obtained only for H_{ac} values $\geq 2 \text{ Oe}$. This is demonstrated more quantitatively in Fig. 3, where the maximum of the imaginary part χ''_{max} is plotted versus the amplitude of the exciting field H_{ac} for a square and a disk both patterned from one and the same film. Clearly, for both sample shapes a

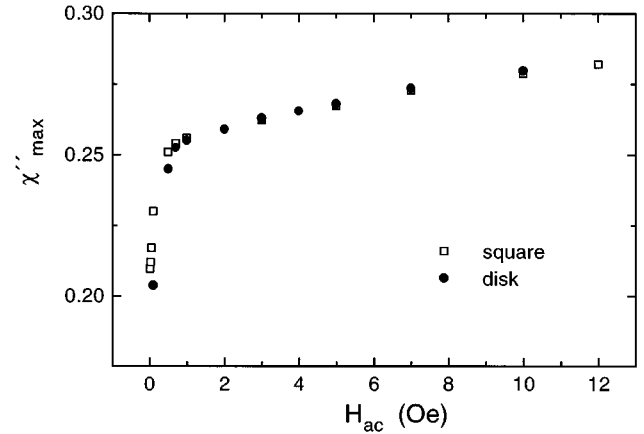


FIG. 3. Maximum value of the imaginary part χ''_{max} as a function of the applied effective magnetic ac field H_{ac} for a square ($2 \times 2 \text{ mm}^2$) and a disk (diameter 1 mm), both patterned from a YBaCuO film.

nearly identical behavior is observed. A steep increase of χ''_{max} for small H_{ac} values is followed by a saturationlike behavior, which, however, still exhibits a significant H_{ac} dependence. This latter regime is attributed to hysteretic Bean-like losses, mainly, as will be shown in the following, because of the good agreement between the experimental χ''_{max} values and those predicted by models based on Bean theory. It should be kept in mind, however, that the premises of the ideal Bean model are in contrast to the observed H_{ac} dependence found in Fig. 3, which, though being small, is experimentally significant. At this point, it is concluded that any experimental test of theories based on the Bean model should be performed applying amplitudes H_{ac} corresponding to χ''_{max} values above the steep increase in Fig. 3, i.e., $H_{ac} \geq 2 \text{ Oe}$. In the following, this criterion was met in all cases. As already mentioned above, the decrease of χ''_{max} for small H_{ac} values is attributed to the growing dominance of screening rather than to a change towards a different loss mechanism. This interpretation is supported by recent theoretical work predicting significantly larger χ''_{max} values in the case of linear flux flow losses²⁸ as compared to hysteretic losses calculated from Bean models.

In the following, the experimental susceptibility results obtained for rectangles, squares, and disks are compared to theories based on the Bean model by plotting the imaginary versus the real parts (Coles-Coles plot). This representation offers the advantage that such a comparison is possible without the explicit knowledge of the critical current density $J_c(T)$ of a specific sample. An example may be given by referring to the strip geometry, for which the magnetic moment can be expressed in terms of geometrical factors, the critical current density and a reduced field h as stated by Eq. (4) above. Applying the hysteretic behavior as given by Eq. (1), which is exact within the Bean model, results in the following expressions for the real and imaginary parts of the susceptibility for a strip:²⁹

$$\chi' = -\frac{1}{h} \tanh h, \quad (8)$$

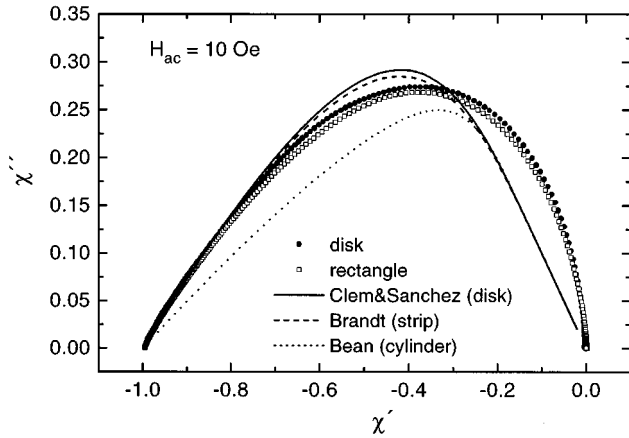


FIG. 4. Coles-Coles plot as obtained from the temperature dependence of the susceptibility determined for a rectangle and a disk both patterned from a YBaCuO film. The corresponding theoretical predictions are added by the symbols defined in the inset.

$$\chi'' = -\frac{1}{h} \tanh h + \frac{2}{h} \tanh \frac{h}{2}. \quad (9)$$

Since $h \propto J_c^{-1}$ with a proportionality constant containing geometrical factors, a test of these expressions necessarily demands the knowledge of J_c . If, however, χ'' is plotted versus χ' , the reduced field h can be treated as a curve parameter with $0 \leq h < \infty$. Any specific sample shape then yields a characteristic curve in the Coles-Coles plot.

The method is demonstrated in Fig. 4, where the imaginary part of the susceptibility is plotted versus the real part for a rectangle ($2 \times 3 \text{ mm}^2$) and a disk (diameter 1 mm) applying an ac amplitude of 10 Oe. The experimental results obtained for the different sample shapes are very similar. For example, the data for a square ($2 \times 2 \text{ mm}^2$) differ from those of the above disk by only 1% or less. Therefore, the disk data were omitted in Fig. 4 for clarity. Especially, the slopes at the low and high temperature end corresponding to $\chi' = -1$ and 0, respectively, are found to be practically independent of the sample shape. The different shapes manifest themselves only in small characteristic variations of the height of the χ'' maximum in agreement with the theoretical predictions, which are also represented in Fig. 4 by a solid and a dashed line. Additionally, the classical prediction of the Bean model for an infinite cylinder in a longitudinal magnetic field is included in the figure by a dotted line. It is obvious that these classical Bean results totally fail to describe the data obtained for thin films of related shape, but with orientations of the external field resulting in strong demagnetizing effects. In contrast, the recent theories adapted to the present samples and field orientations yield an excellent description of the data at the low temperature end. They also correctly predict the observed similarity between the results for both sample shapes including the slightly larger χ''_{max} value for the disk as compared to the rectangle. The magnitude of χ''_{max} , however, is overestimated by theory by approximately 7%. In view of the fact that experimentally χ''_{max} is weakly dependent on H_{ac} pointing to a principal problem of the Bean model, this discrepancy appears to be acceptable. It is worth mentioning that the results found for the square, which are not included in Fig. 4 for clarity, co-

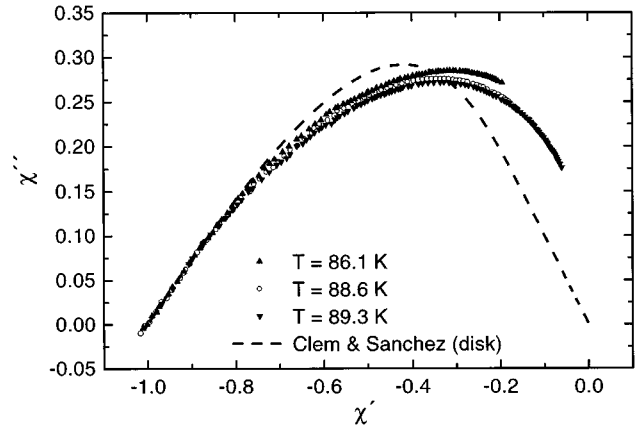


FIG. 5. Isothermal Coles-Coles plots for a disk (same as in Fig. 4) obtained at the temperatures indicated in the inset by varying the magnetic field H_{ac} . For comparison, the theoretical result for a disk is included by the dashed curve.

incide with the disk data within 1.7% over the whole range $-1 \leq \chi' \leq 0$ reflecting the trend given by theory, which predicts an agreement for these two geometries within 0.2%. The theoretical curves also show the same overall asymmetric appearance as the experimental data. There is, however, a significant discrepancy between both at the high temperature end, i.e., for $-0.2 \leq \chi' \leq 0$. The same discrepancy has been reported recently by Stoppard and Guban,²⁹ who attribute it to the growing influence of a field dependence of the critical current density, which is not taken into account by the Bean models and which is expected to predominantly reduce the real part of the susceptibility. Such an interpretation is in accordance with the above-mentioned H_{ac} dependence of χ''_{max} . Nevertheless, alternative loss mechanisms like flux creep, which tends to increase χ'' as compared to the purely hysteretic Bean case,²⁸ could also be responsible for the observed discrepancy in Fig. 4. Furthermore, in view of the results obtained for ring-shaped films, which will be presented in the following section, one might argue that a disk exhibiting J_c inhomogeneities behaves like a ring with some effective diameter and width, again leading to a significant enhancement of χ'' over the corresponding disk values for $-0.2 \leq \chi' \leq 0$.

Before closing this section, there remains a principal point to be checked. As has been shown in the context of Eqs. (8) and (9), the reduced field $h \propto H_{\text{ac}}/J_c(T)$ can be treated as an independent running variable in the Coles-Coles plot. Thus, within the Bean model, there is no difference between measurements keeping the temperature fixed and varying the field amplitude or, as for the data presented so far, keeping H_{ac} constant and varying the temperature. Since, however, the theoretical results were obtained by calculating isothermal hysteresis curves, from which the susceptibility behavior can be deduced, the above equivalence should be experimentally tested. The results of such a test are given in Fig. 5, where again experimental χ'' versus χ' data for a disk (same sample as in Fig. 4) are compared to the corresponding theory. In this case, however, the experimental points were determined at fixed temperatures as attributed to each data set, by varying the amplitude H_{ac} . The same degree of agreement between theory and experiment is observed as described above in the context of Fig. 4 demonstrating the

equivalence of both experimental procedures as suggested theoretically. For example, the weak dependence of χ''_{\max} on H_{ac} as observed in Fig. 4 is translated into a weak temperature dependence of this property in Fig. 5, simply because here at the different temperatures different ac fields have to be applied to obtain χ''_{\max} .

B. Rings

In the following, the limit of a thin narrow ring will be discussed with width w much smaller than the mean radius R , $R - w/2 \leq r \leq R + w/2$. The virgin magnetization curve of such a ring is composed of two straight lines,

$$\begin{aligned} m(H_a) &= (H_a/H_p)m_{\text{sat}}, & H_a \leq H_p, \\ m(H_a) &= m_{\text{sat}}, & H_a \geq H_p. \end{aligned} \quad (10)$$

This is so since the screening supercurrent in the ring is limited to a maximum value $I_c = J_c dw$. As long as the current I induced in the ring by the applied field H_a is $I < I_c$, no magnetic flux can penetrate through the ring into the hole of the ring. When $I = I_c$ is reached, the ring becomes transparent to magnetic flux. Therefore, when the applied field is increased further, flux lines will move through the ring as described in Ref. 11. The flux lines transport magnetic flux into the ring hole until the screening current has decreased again to the value I_c . The magnetic moment $m = \pi R^2 I$ of the ring thus saturates to the value

$$m_{\text{sat}} = \pi R^2 I_c. \quad (11)$$

The applied field value H_p at which this saturation is reached follows from the inductivity L of the flat ring,³⁰

$$L = \mu_0 R \left(\ln \frac{8R}{w} - \frac{1}{2} \right). \quad (12)$$

For comparison, the inductivity of a ring made of a wire with diameter $w \ll R$ is^{30,31}

$$L = \mu_0 R \left(\ln \frac{8R}{w} - 2 \right). \quad (13)$$

The magnetic flux generated in the ring hole by a ring current I is $\phi = LI$. As long as $I < I_c$ one has ideal screening, thus $\phi = -\pi R^2 \mu_0 H_a$. Equating these two fluxes one obtains, for the flat ring,

$$I = \phi/L = \frac{-\pi R}{\ln(8R/w) - 1/2} H_a. \quad (14)$$

At $H_a = H_p$ one has reached $I = I_c = J_c w d$, thus

$$H_p = \frac{\ln(8R/w) - 1/2}{\pi R} I_c. \quad (15)$$

The slope of $m(H_a)$ for $H_a < H_p$ is therefore

$$m'(0) = -\frac{m_{\text{sat}}}{H_p} = -\frac{\pi^2 R^3}{\ln(8R/w) - 1/2}. \quad (16)$$

Formulas (10)–(16) are accurate to corrections of order $w/2R$ since the precise values of m and L depend on the

current distribution across the ring width w , which changes during the magnetization process.

With prescription (1) the virgin magnetization curve (10) yields hysteresis loops in the shape of parallelograms.^{32,33} From these loops one obtains the complex susceptibility $\chi = \chi' - i\chi''$ of a superconducting ring within the Bean model. For a cycled magnetic field $H_a(t) = H_0 \sin(\omega t)$ one defines

$$\chi(H_0) = \frac{\omega}{\pi H_0} \int_0^{2\pi} m(t) e^{-i\omega t} dt. \quad (17)$$

Note that this *nonlinear* susceptibility does not depend on the frequency $\omega/2\pi$ if $m(t)$ is taken from the Bean model, but it depends on the sweep amplitude H_0 . In contrast, the *linear* susceptibility of an ohmic conductor or of any conductor with linear complex resistivity (e.g., a superconductor above the depinning line) depends on ω but not on H_0 . More precisely, the definition (17) requires that in it ω coincides with the ω of the applied field or with an integer multiple of it; here we do not consider the higher harmonic responses χ_n , $n = 2, 3, 4, \dots$, but only the fundamental response $\chi_1 = \chi$.

From Eqs. (1), (10), and (17) one obtains the susceptibility of the ring normalized to the initial value $\chi(0) = -1$, i.e., to $\chi \rightarrow -\chi/m'(0)$,

$$\chi'(h) = -1,$$

$$\chi''(h) = 0, \quad h \leq 1,$$

$$\chi'(h) = -\frac{1}{2} - \frac{1}{\pi} \arcsin s - \frac{1}{\pi} s \sqrt{1-s^2},$$

$$\chi''(h) = \frac{4}{\pi} \frac{h-1}{h^2} = \frac{1-s^2}{\pi}, \quad h \geq 1, \quad (18)$$

with $h = H_0/H_p$ and $s = 2/h - 1$.

Interestingly, with the ring susceptibility (17) the polar plot χ'' versus χ' with h as parameter is *symmetric*, i.e., $\chi''(\chi')$ yields the same curve as $\chi''(-1-\chi')$. The maximum of the dissipative part of the ring susceptibility $\chi''_{\max} = 1/\pi = 0.318$ occurs at $h = 2$ (at $s = 0$). For large amplitudes $h = H_0/H_p \gg 1$ one has $\chi'(h) \approx -1.69/h^{3/2}$ and $\chi''(h) \approx 4/\pi h$.

A similar result has been obtained previously by Ishida and Mazaki.³⁴ Modeling a Josephson network by an effective superconducting ring containing one weak link, they calculated the response of such a ring to an external magnetic ac field assuming that above a maximum field amplitude H_m corresponding to the critical current density of the weak link, magnetic flux quanta can penetrate the ring. The resulting real and imaginary parts of the susceptibility can be shown to be equivalent to Eq. (18) if one puts $H_p = H_m$, i.e., the critical current introduced in Eq. (15) could as well be interpreted as the critical current of one effective weak link, or of several such weak links, which might be present in the patterned ring due to twin boundaries.

As in Eq. (18), to calculate the temperature dependence of χ' and χ'' for a given amplitude H_{ac} from the Ishida-Mazaki model, a knowledge of the detailed $J_c(T)$ behavior is neces-

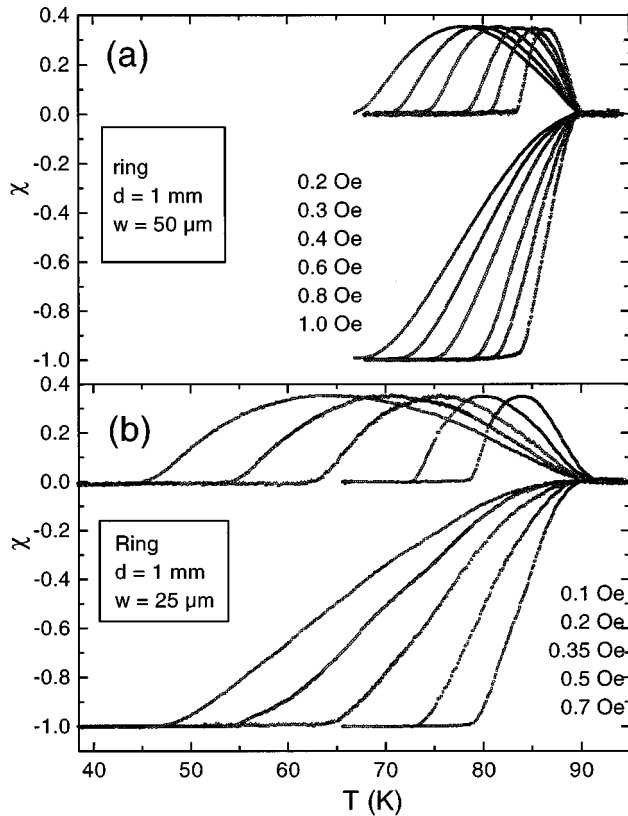


FIG. 6. Influence of the effective magnetic ac field as given in the insets on the temperature dependence of the susceptibilities of two rings with a width of (a) $50 \mu\text{m}$ and (b) $25 \mu\text{m}$, both patterned from a YBaCuO film. The attribution of the fields to the curves is from right to left starting with lowest H_{ac} value, the temperature scale is the same in (a) and (b).

sary in contrast to χ'' versus χ' plots, which allow a test of the geometry dependence without this input.

In Fig. 6 the original data sets for the temperature dependence of the real and imaginary parts of the susceptibility of two different rings ($w = 50 \mu\text{m}$ and $25 \mu\text{m}$) are shown as obtained for various ac amplitudes. Three main features should be noted. First, there is the already discussed shifting of the temperature T^* , below which perfect screening is obtained, towards lower values by increasing H_{ac} . This behavior is due to the increasing currents necessary to screen larger ac amplitudes and which can be carried only at lower temperatures. In the ring with the smaller width, to screen a given value of H_{ac} , the resulting larger current densities lead to a correspondingly lower temperature T^* as observed in Fig. 6. Second, a comparison to the corresponding curves obtained for disks (cf. Fig. 2) indicates a significantly different shape of the χ'' peaks observed for rings. Third, the peak heights are independent of H_{ac} , in agreement with the Bean model given above. To test this model further, in Fig. 7 the corresponding χ'' versus χ' plots are presented for rings with different widths. Added to this figure is the theoretical result according to Eq. (18) as well as the previous data for a disk allowing to demonstrate the striking symmetry difference of the χ'' versus χ' curves between rings and disks as predicted by theory. Clearly, all three rings with widths of $10 \mu\text{m}$, $25 \mu\text{m}$, and $50 \mu\text{m}$ behave identically within the experimental resolution and exhibit the predicted symmetry, i.e., $\chi''(\chi')$

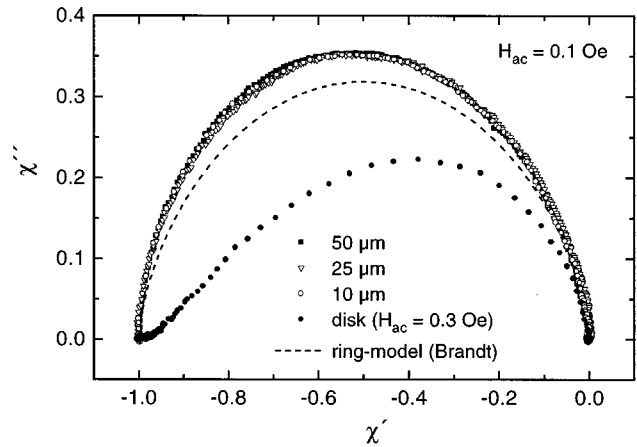


FIG. 7. Coles-Coles plots for rings of varying widths as given in the inset, which all were patterned from different YBaCuO films. For comparison, experimental data for a disk as well as the theoretical result for a ring are included.

and $\chi''(-1-\chi')$ yield the same curve. Furthermore, the high and low temperature slopes of this curve are correctly described by theory, while the absolute height of the experimentally observed χ'' maxima is larger than the theoretical value of $1/\pi$ by approximately 10%.

In order to study the transition from a disk to a ring behavior in more detail, rings of different widths were patterned sequentially from one YBaCuO film starting with the corresponding disk (radius $500 \mu\text{m}$). The results are shown in Fig. 8, again in the form of χ'' versus χ' plots. While at the high temperature side ($-0.2 < \chi' < 0$) all samples exhibit a ringlike behavior, the different symmetry of the curves clearly can be distinguished at lower temperatures. The disk as well as the ring with the largest width of $400 \mu\text{m}$ both show practically the same χ'' versus χ' curves. For the ring with $w = 350 \mu\text{m}$, however, already a significant deviation from the theoretically expected disk behavior is observed within the range of $-0.8 < \chi' < -0.4$. These deviations become continuously stronger for rings with smaller widths until, for rings with $w \leq 100 \mu\text{m}$, the perfectly symmetric χ'' versus χ' curves of ideal rings are obtained.

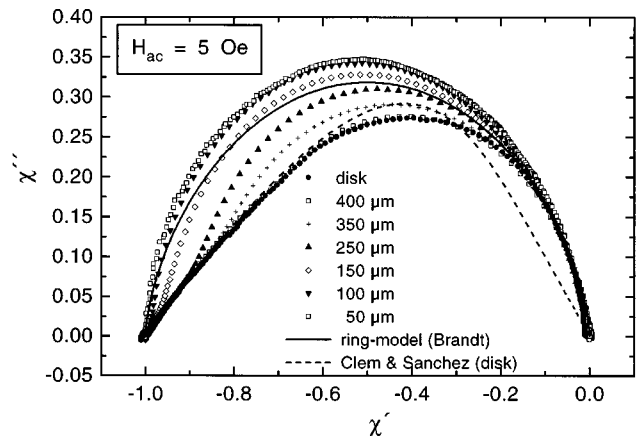


FIG. 8. Coles-Coles plots for rings of varying widths as indicated in the inset. The rings are all patterned from the same YBaCuO film starting with a disk of diameter 1 mm , the data of which are given by closed circles. Included are the corresponding theoretical results.

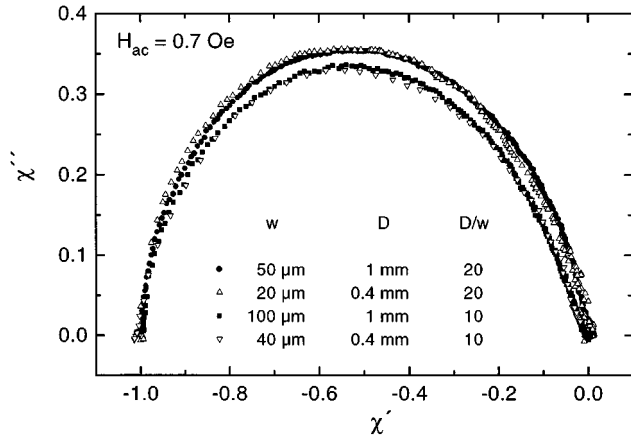


FIG. 9. Coles-Coles plots for rings of varying diameter D as well as widths w as indicated in the inset. Different rings with identical D/w results in the same χ'' -vs- χ' curves.

Two remarks seem to be in order with respect to the overall behavior of the transition from a disk to a ring presented in Fig. 8. The common ringlike behavior of all samples at the high temperature end suggests that even in a disk the current flow is restricted to an effective ringlike path close to T_c . This could be caused by inhomogeneities of the critical current density, in which case the effective ring corresponds to the path of highest J_c at a fixed temperature. At low temperatures, except for the rings with the smallest widths, all samples start with a common slope, which is theoretically expected for a disk. This may be attributed to the fact that the broader rings allow an inhomogeneous penetration of magnetic flux corresponding to an inhomogeneous current distribution starting from the outer diameter, while the current within rings with small widths can be approximated very well by the idealization of a constant homogeneous distribution. Thus, it appears that there is a critical width of the rings below which their behavior can be approximated by the above ideal model. Up to here, only rings with an outer diameter of $D=1$ mm have been studied. On the other hand, one intuitively expects a critical ratio D/w rather than an absolute value of w below which the ideal ring behavior sets in. To test this, additional rings with $D=0.4$ mm were prepared and the corresponding results are shown in Fig. 9. Clearly, rings with the same D/w ratio exhibit identical χ'' versus χ' curves within the experimental resolution and for $D/w \geq 20$ the ideal ring behavior of above is approached with $\chi''_{\max} = 0.35$, while for $D/w=10$ the value of χ''_{\max} already is significantly lower, though the curves are still symmetric as typical of rings. Thus, it is concluded that the ratio D/w is the essential parameter to separate disk from ring behavior.

Referring to Eq. (15) it is clear that the critical current $I_c(T)$ can be determined from the susceptibility of an ideal ring, if the penetration field H_p is measured at a fixed temperature T and the ring radius and width are known. Furthermore, Eq. (18) shows that for $H_{ac}=H_p$, i.e., for $h=1$, a value of $\chi''(1) = 0$ results, suggesting the following procedure to determine H_p . For a given ring with R and w , the temperature dependence of the susceptibility is measured with an ac amplitude H_{ac} . Coming from the low temperature side, at T^* as defined above, the imaginary part starts to

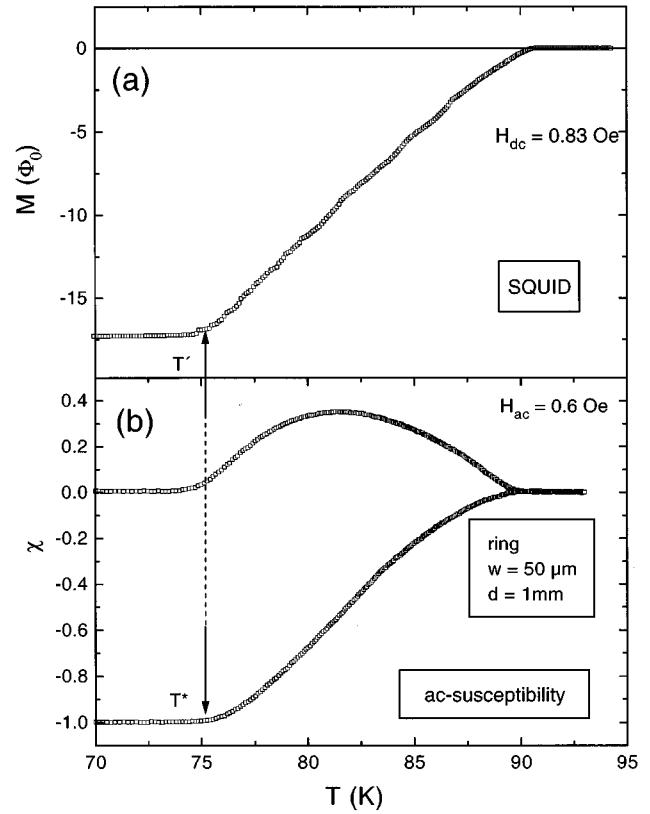


FIG. 10. (a) Temperature dependence of the magnetic moment of a YBaCuO ring (diameter 1 mm), which had been zero-field cooled to $T \leq T_c$ and then exposed to a magnetic field of $H_{dc} = 0.83$ Oe. The data are taken on warming by a SQUID magnetometer and are given in units of flux quanta Φ_0 . At T' the shielding currents approach the critical current of the ring. (b) Temperature dependence of the susceptibility for the same ring as in (a) taken with an ac amplitude of 0.85 Oe. In both cases the fields are directed parallel to the ring axis.

deviate from zero allowing the identification $H_p(T^*)=H_{ac}$. To test this procedure, a ring with $R=0.5$ mm and $w=50$ μm was mounted in a SQUID magnetometer with its normal parallel to the direction of an external magnetic field H_{dc} . After zero-field cooling (ZFC) to 5 K, an external field of $H_{dc}=0.83$ Oe is switched on leading to superconducting shielding currents. The corresponding magnetic moment of the ring is determined by the SQUID. After the field switching, the temperature is increased. As long as the shielding currents are below the critical current density $J_c(T)$ of the ring, the SQUID signal remains constant during the warm up until at T' the critical current density is reached. Thus, for temperatures above T' the ring can carry only smaller currents resulting in a decrease of the SQUID signal leading to a well-pronounced kink at T' . This behavior is demonstrated in Fig. 10(a), where the SQUID signal is given in units of a flux quantum Φ_0 . In Fig. 10(b) the corresponding susceptibility behavior of the same ring is presented as obtained for an effective ac field of 0.6 Oe corresponding to an amplitude of 0.85 Oe. Clearly, χ'' starts to deviate from zero at a well-defined temperature T^* as indicated in the figure. The important point here is that the temperatures T^* and T' coincide within the experimental uncertainties as demonstrated by the vertical dashed line. This proves that the above-suggested

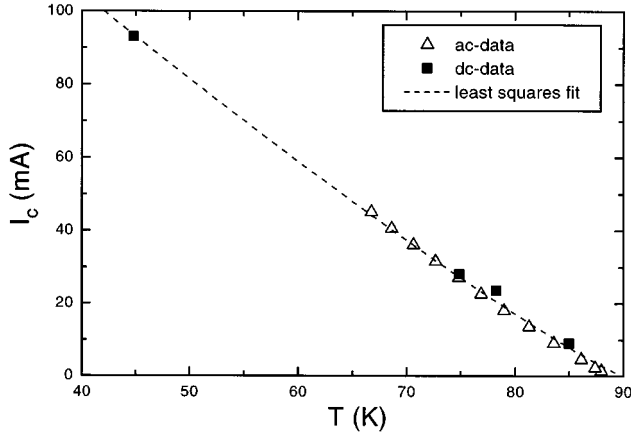


FIG. 11. Critical currents of the same ring as in Fig. 10 as determined either from SQUID data (closed squares) or susceptibility measurements (open triangles). Both data sets can be described by a power law $I_c(T) \propto (1 - T/T_c)^\beta$ with $\beta = 1.1$ as extracted from a least squares fit given in the figure by the dashed curve.

procedure to determine I_c from ac-susceptibility measurements on thin narrow rings is sound.

For a quantitative comparison between the SQUID and the susceptibility measurements, the SQUID signal must be first determined as a function of the current flowing in the ring. Such a calibration can be obtained by applying different fields H_{dc} after ZFC to a low enough fixed temperature and plotting the resulting magnetic moment as given by the SQUID after warming to T_c in units of Φ_0 versus H_{dc} . If the inductance L of the ring is known, the slope of the resulting straight line can be expressed in terms of flux quanta per mA of the current flowing in the ring. For the above example presented in Fig. 10, this calibration factor is $1.56 \Phi_0/\text{mA}$ using the inductance as given by Eq. (12) and the ring dimensions $R = 500 \mu\text{m}$ and $w = 50 \mu\text{m}$. Applying this method, the temperature dependence of the critical currents $I_c(T)$ has been observed as presented in Fig. 11. Here, the results obtained by the SQUID technique are given by the closed squares. Added to this figure are the results obtained by the susceptibility procedure (open triangles) using the same inductance as above and the solid line is a fit to the results with a power law of the form $I_c(T) \propto (1 - T/T_c)^\beta$ yielding $\beta = 1.1$. The agreement of both data sets convincingly corroborates the validity of the ac procedure.

The equivalence of the present model for a thin narrow ring and the theory by Ishida and Mazaki already has been mentioned. This can be exploited to test their prediction on the behavior of higher harmonics of the susceptibility as a function of temperature. For this purpose, the real and imaginary parts of the third harmonic of rings with different width were especially analyzed.

According to Ishida and Mazaki,^{34,35} the real and imaginary parts of the third harmonic of their ring model is given by

$$\chi_3' = \frac{1}{12\pi} (\sin 4\alpha - 2 \sin 2\alpha), \quad (19)$$

$$\chi_3'' = -\frac{1}{12\pi} (\cos 4\alpha - 2 \cos 2\alpha + 1) \quad (20)$$

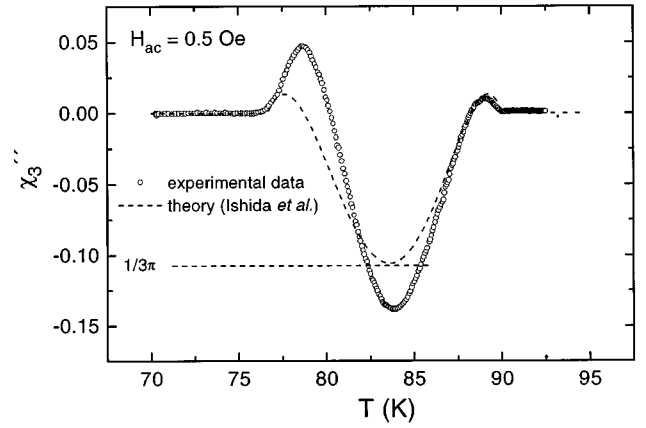


FIG. 12. Temperature dependence of the imaginary part of the third harmonic χ_3'' obtained for a YBaCuO ring (diameter 1 mm, width $50 \mu\text{m}$). The dashed line represents a theoretical result due to Ishida and Mazaki adjusted to the experiment by assuming the same power law for $I_c(T)$ as in Fig. 11, using the experimental $T_c = 90 \text{ K}$ and the fitting parameter $H_m(T=0) = 5.7$.

with $\alpha = 2 \arcsin(H_m/H_{ac})^{1/2}$, where the maximum field H_m is proportional to the critical current density $J_c(T)$ of the ring. With the same power law for $J_c(T)$ as above and taking $H_m(T=0)$ as the only fitting parameter while for T_c and the exponent β the experimentally found values are used, one is able to calculate the third harmonic and to compare it to the experimental results. This is demonstrated for a ring with $R = 500 \mu\text{m}$ and $w = 50 \mu\text{m}$ in Fig. 12, where the experimental results for the real and imaginary parts of the third harmonic are presented together with the theoretical values obtained by adjusting $H_m(T=0)$. Comparison shows that theory and experiment agree only qualitatively. For instance, both exhibit two characteristic positive peaks, one just below T_c and the other at approximately 78 K, and a negative dip between them. In theory, however, the behavior is symmetric relative to the minimum, while experimentally a clear asymmetry can be observed with an enhancement of the peak at the low temperature side. In addition, the magnitude of the minimum of the experimental $\chi_3''(T)$ curve significantly exceeds the theoretical value of $-1/3\pi$ obtained at $\alpha = \pi/2$. Due to the higher sensitivity of the third harmonic, both deviations magnify the differences between theory and experiment, which were already observed for the fundamental susceptibility curves, i.e., the higher χ_{max}'' value of the experimental data as well as their slight asymmetry.

Though the theoretical $\chi_3''(T)$ curves give no quantitative description of the experiment, their characteristic structure with two positive peaks can be used to monitor the transition of the susceptibility behavior from one typical of a disk to that of a ring. This is demonstrated in Fig. 13, where the imaginary part $\chi_3''(T)$ is presented for a disk, out of which rings were successively patterned with different widths. Clearly, while the disk exhibits a minimum with only a small peak at the high temperature side, a second peak evolves for rings with decreasing widths. In all cases, however, the already mentioned asymmetry with a more pronounced peak at the low temperature side, is observed.

IV. SUMMARY AND CONCLUSION

The real and imaginary parts of the ac susceptibility of differently shaped thin $\text{YBa}_2\text{Cu}_3\text{O}_{7-\delta}$ films as a function of

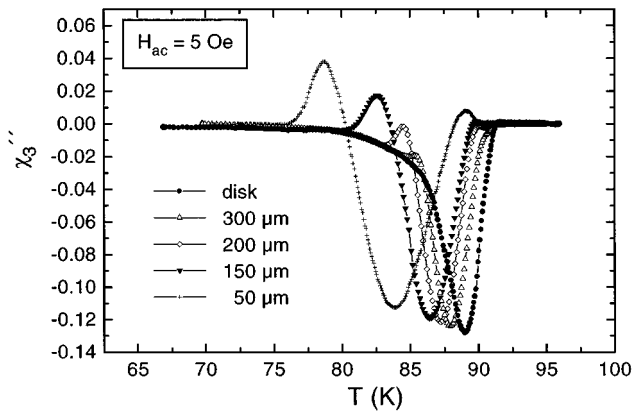


FIG. 13. Temperature dependence of the imaginary part of the third harmonic χ_3'' obtained for rings of different widths as given in the inset. The rings are all patterned from the same YBaCuO film starting with a disk of diameter 1 mm, the data of which are given by closed circles.

temperature have been presented and compared with corresponding theories for the case of the exciting magnetic field being perpendicular to the sample surface. In accordance with the theoretical expectation, only small differences are observed between the results for rectangles, squares, and disks. Thus, the main emphasis is given to the behavior of disks and rings. To test the theories without specific assumptions on, e.g., the temperature dependence of the critical current density, plots of the imaginary versus the real part of the susceptibility turn out to be especially useful. It is found that the present state-of-the-art theories based on the Bean model yield much better descriptions of the investigated perpendicular field geometries than the previous longitudinal approximations. At the low temperature side below the maximum of χ'' , the agreement between theory and experiment is even quantitative, while for temperatures close to T_c striking differences can be observed, which are attributed mainly to a field dependence of J_c as well as to non-hysteretic loss mechanisms. It could also be demonstrated that χ'' versus χ' plots determined either by varying the temperature at a fixed magnetic field or by varying the field at constant temperature are equivalent. Since theory predicts a significant change of the χ'' versus χ' curves from an asymmetric be-

havior for disks to a symmetric one for ideal narrow rings, this transition has been studied in more detail and could be experimentally confirmed. For rings, the theoretical predictions are quantitative for temperatures close to T_c , where rings and disks show a common behavior, while at lower temperatures deviations of the experimentally determined imaginary parts are found towards higher values. Additionally, the ratio of the diameter to the width of a ring turned out to be the main parameter characterizing its susceptibility behavior. Independent measurements on rings with a SQUID magnetometer allowed to test a procedure based on the ac response of rings to quantitatively extract their critical currents as a function of temperature. Good agreement between the corresponding ac and dc data were obtained. Finally, the prediction of Ishida and Mazaki concerning the third harmonic response of a narrow ring to an ac field was tested. Though the theory allows no quantitative description of the experimental results, it turned out that specific structures of the imaginary part $\chi_3''(T)$, which are characteristic of rings and are not present in disks, can be used for studying the transition from the susceptibility behavior of a disk towards that of an ideal narrow ring.

Detailed computations of ac susceptibilities of thin disks and rings in a perpendicular field are given in Ref. 36 for the Bean model ($J_c = \text{const}$), the Kim model [$J_c(B) \propto (|B| + B_1)^{-1}$], and for various degrees of flux creep characterized by power-law current-voltage curves.

In summary, we conclude that due to the improved control of the quality and the geometry of thin film samples, a test of the state-of-the-art theories based on the Bean model and describing the ac response in the more complex situation with the magnetic field perpendicular to the film surface has been made possible. The overall results demonstrate the significant improvement of these theories, though a quantitative agreement over the full temperature range of the susceptibility data below T_c has still not been obtained.

ACKNOWLEDGMENTS

The experimental assistance by A. Feucht, J. Häring, and Th. Theilig is gratefully acknowledged. In part, this work was financially supported by a Landesschwerpunkt Baden-Württemberg.

¹ A. M. Campbell, *J. Phys. C* **2**, 1492 (1969).

² C. P. Bean, *Phys. Rev. Lett.* **8**, 250 (1962); *Rev. Mod. Phys.* **36**, 31 (1964).

³ P. W. Anderson and Y. B. Kim, *Rev. Mod. Phys.* **36**, 39 (1964).

⁴ T. Ishida and R. B. Goldbarb, *Phys. Rev. B* **41**, 8937 (1990).

⁵ A. M. Campbell and J. E. Evetts, *Adv. Phys.* **21**, 199 (1972).

⁶ R. A. Hein, *Phys. Rev. B* **33**, 7539 (1986).

⁷ *Magnetic Susceptibility of Superconductors and Other Spin Systems*, edited by R. A. Hein, Th. L. Francavilla, and D. H. Liebenberg (Plenum Press, New York, 1991).

⁸ G. Blatter, M. V. Feigel'man, V. B. Geshkenbein, A. I. Larkin, and V. M. Vinokur, *Rev. Mod. Phys.* **66**, 1125 (1994).

⁹ E. H. Brandt, *Rep. Prog. Phys.* **58**, 1465 (1995).

¹⁰ E. H. Brandt, M. Indenbom, and A. Forkl, *Europhys. Lett.* **22**, 735 (1993).

¹¹ E. H. Brandt and M. Indenbom, *Phys. Rev. B* **48**, 12 893 (1993).

¹² E. Zeldov, J. R. Clem, M. McElfresh, and M. Darwin, *Phys. Rev. B* **49**, 9802 (1994).

¹³ P. N. Mikheenko and Yu. E. Kuzovlev, *Physica C* **204**, 229 (1993).

¹⁴ J. Zhu, J. Mester, J. Lockhart, and J. Turneaure, *Physica C* **212**, 216 (1993).

¹⁵ J. R. Clem and A. Sanchez, *Phys. Rev. B* **50**, 9355 (1994).

¹⁶ G. Linker, X. X. Xi, O. Meyer, Q. Li, and J. Geerk, *Solid State Commun.* **69**, 249 (1989).

¹⁷ R. Huber, M. Schneider, U. Wagner, and P. Ziemann, *J. Alloys Compd.* **195**, 255 (1993).

- ¹⁸ G. Ziebold and D. Korn, J. Phys. E **12**, 490 (1979).
- ¹⁹ Ch. Neumann, P. Ziemann, J. Geerk, and X. X. Xi, Physica C **162/164**, 321 (1989).
- ²⁰ W. T. Norris, J. Phys. D **3**, 489 (1970); Y. Yang, T. Hughes, C. Beduz, D. M. Spiller, R. G. Scurlock, and W. T. Norris, Physica C **256**, 378 (1996).
- ²¹ E. H. Brandt, Phys. Rev. Lett. **74**, 3025 (1995).
- ²² E. H. Brandt, Phys. Rev. B **52**, 15 442 (1995).
- ²³ A. Forkl, Phys. Scr. **T49**, 148 (1993).
- ²⁴ E. H. Brandt, Phys. Rev. B **54**, 4246 (1996).
- ²⁵ Ch. Heinzl, Ch. Neumann, and P. Ziemann, Europhys. Lett. **13**, 531 (1990).
- ²⁶ M. Tinkham, *Introduction to Superconductivity* (McGraw-Hill, New York, 1975).
- ²⁷ M. Avirovic, Ch. Neumann, P. Ziemann, J. Geerk, and H. C. Li, Solid State Commun. **67**, 795 (1988).
- ²⁸ E. H. Brandt, Physica C **235-240**, 2939 (1994).
- ²⁹ O. Stoppard and D. Guban, Physica C **241**, 375 (1995).
- ³⁰ J. Gilchrist and E. H. Brandt, Phys. Rev. B **54**, 3530 (1996).
- ³¹ L. D. Landau and E. M. Lifshitz, *Electrodynamics of Continuous Media* (Pergamon, Oxford, 1963), Vol. III.
- ³² Such parallelograms are also obtained in rings with a weak link and in other models; see the discussion by Gilchrist (Ref. 33) and the references therein.
- ³³ J. Gilchrist and M. Konczykowski, Physica C **212**, 43 (1993).
- ³⁴ T. Ishida and H. Mazaki, J. Appl. Phys. **52**, 6798 (1981).
- ³⁵ T. Ishida and H. Mazaki, Phys. Lett. **87A**, 373 (1982).
- ³⁶ E. H. Brandt, Phys. Rev. B **55**, 14 513 (1997).